Blue-Green Systems

IWA PUBLISHING

18

Blue-Green Systems Vol 1 No 1
doi: 10.2166/bgs.2019.198

Fabrication of a novel cyanoethyl cellulose substrate for thin-film composite forward osmosis membrane

Ke Zheng[a,b] and Shaoqi Zhou[a,b,c,d,*]

[a] School of Civil Engineering and Transportation, South China University of Technology, Guangzhou 510641, China

[b] School of Environment and Energy, South China University of Technology, Guangzhou Higher Education Mega Center, Guangzhou 510006, China

[c] Guizhou Academy of Sciences, Shanxi Road 1, Guiyang 550001, China

[d] State Key Laboratory of Subtropical Building Science, South China University of Technology, Guangzhou 510641, China

*Corresponding author. E-mail: fesqzhou@scut.edu.cn

Abstract

In this study, cyanoethyl cellulose (CEC) was used as a membrane material, and polyvinylpyrrolidone (PVP) was used as pore-forming agent to prepare the substrates for the thin-film composite (TFC) forward osmosis (FO) membrane for the first time. The experimental results demonstrate that the properties of the substrates were significantly improved after PVP was added. The scanning electron microscope (SEM) images show that a two-sublayer structure, a fringe-like top sublayer and macrovoids with sponge-like wall bottom sublayer, were formed after the addition of PVP. These improvements contributed to improved membrane performance during FO tests. Meanwhile, after adding PVP, the TFC membranes exhibited good water flux, and excellent specific reverse salt flux. For instance, the TFC-M2 exhibited 9.10/20.67 LMH water flux, 1.35/2.24 gMH reverse salt flux, and 0.15/0.11 g/L specific reverse salt flux in FO/pressure-retarded osmosis mode while using 1 M NaCl as the draw solution and deionized (DI) water as the feed solution.

Key words: cyanoethyl cellulose, forward osmosis, polyvinylpyrrolidone, substrate, thin-film composite membrane

NOMENCLATURE

A	water permeability
B	salt permeability
S	structure parameter
ε	porosity
r_m	average pore size
CEC	cyanoethyl cellulose
DS	draw solution
FS	feed solution
FO	forward osmosis
ICP	internal concentration polarization
PRO	pressure-retarded osmosis
PWP	pure water permeability

Blue-Green Systems Vol 1 No 1
doi: 10.2166/bgs.2019.198

PVP polyvinylpyrrolidone
RSF reverse salt flux
SRSF specific reverse salt flux
TFC thin-film composite

INTRODUCTION

Because of the shortage of freshwater resources, seawater desalination and wastewater treatment have become important issues (Elimelech & Phillip 2011). Thus, forward osmosis (FO) technology, a potential technology for seawater desalination and wastewater treatment, has gained significant attention in recent decades (Akther *et al.* 2015; Qasim *et al.* 2015; Chekli *et al.* 2016; Lu *et al.* 2016a). Moreover, besides seawater desalination and wastewater treatment, the FO process could have applications in the enrichment of liquid foods or pharmaceuticals and osmotic power generation (Ling & Chung 2011; Altaee *et al.* 2015; Sant'Anna *et al.* 2016; Ansari *et al.* 2017). Unlike reverse osmosis (RO) and nanofiltration (NF), which use high hydraulic pressures to separate the solvents and solutes, FO utilizes the osmotic pressure difference between the low-osmotic-pressure feed solution (FS) and high-osmotic-pressure draw solution (DS) to drive water across the FO membrane (Chekli *et al.* 2016). Furthermore, the FO process has distinct advantages, such as low energy consumption, excellent separating precision, and reversible membrane fouling (Qasim *et al.* 2015).

An ideal FO membrane should have a high water flux and limited reverse salt flux (RSF). However, FO performance is severely hindered by the inevitable internal concentration polarization (ICP) that occurs during the FO process (Qasim *et al.* 2015; Wang & Xu 2015; Bui & McCutcheon 2016; Heikkinen *et al.* 2017). Meanwhile, structure parameter (*S* value) is used to reflect the ICP degree in the FO process (Huang *et al.* 2019). Generally, lower S value reflects slighter ICP, which means better FO performance for the membrane (Zheng *et al.* 2018a). Compared to asymmetric FO membranes, thin-film composite (TFC) membranes exhibit better performance for the FO process (Chekli *et al.* 2016). Numerous substrate optimization studies have been published in recent years, and the membrane substrate is known to play an important role in controlling the performance of TFC FO membranes. Consequently, improving the performance of TFC FO membranes remains a hot research topic. The first basic strategy to increase FO performance is to modify the pore morphology of the substrate by adding pore-forming agents (Chen *et al.* 2017c). LiCl, $ZnCl_2$, ethylene glycol (EG), ethanol, polyethylene glycol (PEG), and polyvinyl pyrrolidone (PVP) are common pore-forming agents (Emadzadeh *et al.* 2014; Morales-Torres *et al.* 2016; Wu *et al.* 2016; Chen *et al.* 2017c). Recently, Morales-Torres *et al.* (2016) illustrated that the pore-forming agent PVP could form larger and elongated finger-like pores across membrane substrates. As such, PVP can significantly improve the pore morphology and hydrophilicity of membrane substrates. Wu *et al.* (2016) used PEG as a pore-forming agent to optimize the hydrophilicity, porosity, and pore size of the TFC FO membrane substrates. Their results showed that an FO membrane prepared with 6 wt.% PEG-400 yielded the best FO performance. In addition, alternative methods such as blending hydrophilic polymers or nanoparticles with basic membrane substrate materials are becoming attractive to enhance the hydrophilicity of the substrates and reduce the ICP during the FO process (Zhou *et al.* 2014; Ghanbari *et al.* 2015a; Lu *et al.* 2016a, 2016b; Zhang *et al.* 2016). Zhou *et al.* (2014) blended sulfonated poly(phenylene oxide) (SPPO) with polysulfone to fabricate hydrophilic substrates. The results demonstrated that SPPO alleviated the ICP during the FO process and improved the membrane performance. Ghanbari *et al.* (2015a) illustrated that addition of hydrophilic halloysite nanotubes into the substrates improved the overall porosity, mean pore size, and hydrophilicity of the blended substrates and reduced the S value of the substrate. Lu *et al.* (2016b) reported that layered double hydroxide nanoparticles (LDH-NPs) could be successfully introduced into FO membrane substrates. After adding 2 wt.% LDH-NPs, the water flux became 18.1 LMH at

Blue-Green Systems Vol 1 No 1
doi: 10.2166/bgs.2019.198

1 M NaCl as DS and deionized (DI) water as FS under FO mode, which is 42.5% higher than the pristine FO membrane.

Because cellulose is the most abundant natural polymer in the world, cellulose and its derivatives are widely used (Teramoto 2015). In particular, cellulose acetate (CA) and cellulose triacetate (CTA) are suitable materials for membrane fabrication because of their moderate flux, excellent separating precision, mechanical robustness, and nontoxicity (Qasim *et al.* 2015; Li *et al.* 2016; Chen *et al.* 2017a; Liu *et al.* 2017). However, CA and CTA are being gradually replaced by other artificial polymers, such as polysulfone (PSF), polyether sulfone (PES), polyacrylonitrile (PAN), and polyvinylidene fluoride (PVDF), mainly because both CA and CTA undergo hydrolysis and biodegradation (Qasim *et al.* 2015). However, another cellulose derivative, cyanoethyl cellulose (CEC), exhibits excellent physical and chemical properties, such as increased thermal resistance, excellent mechanical properties, and, especially, microbiological resistance (Zhou *et al.* 2010; Joshi *et al.* 2017). Therefore, CEC is an excellent candidate membrane material.

In this study, the potential of CEC for the fabrication of substrates for TFC FO membranes was investigated. PVP was used as the pore-forming agent and added to the casting solutions. The influence of PVP on the CEC substrates properties in terms of pure water permeability, contact angle, membrane thickness, porosity, average pore size, mechanical strength, and membrane morphology was systematically investigated. In addition, the mechanism of the effect of the pore-forming agent on the active layer properties is demonstrated. The FO performances of CEC-substrate FO membranes with different PVP contents were studied, and the FO performances of the CEC-substrate FO membranes were compared to different FO membrane substrates. This is the first report concerning the application of CEC to the fabrication of FO membranes substrates.

EXPERIMENTAL

Materials

Cyanoethyl cellulose (CEC) powders (substitution degree of 2.6, the chemical structure is shown in Figure 1), polyvinyl pyrrolidone K30 (PVP K30), and *N*,*N*-dimethylacetamide (DMAc) were purchased from Aladdin and used to fabricate the membrane substrates. *m*-Phenylenediamine (MPD) with >99% purity was purchased from Sigma-Aldrich, and trimesoyl chloride (TMC) of >98% purity was purchased from Alfa Aesar; these were used as the monomers for interfacial polymerization (IP). *n*-Hexane with >99% purity from Aladdin was utilized as the solvent for TMC. Reagent grade sodium chloride (NaCl) supplied by Aladdin was used to prepare the DS.

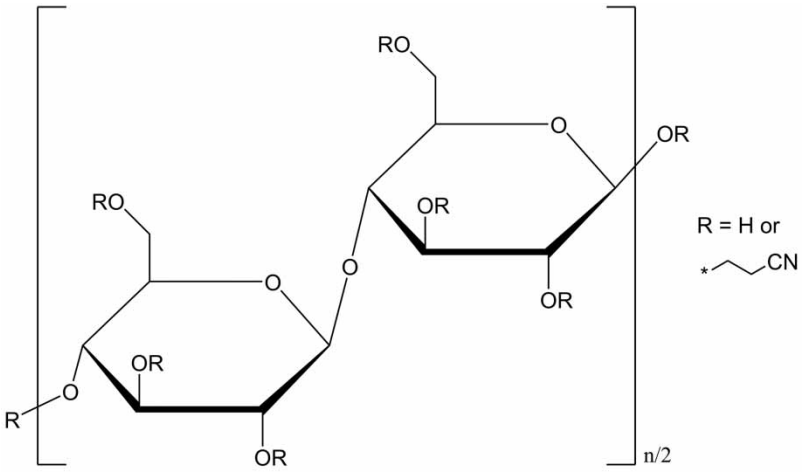

Figure 1 | The chemical structures of cyanoethyl cellulose.

Blue-Green Systems Vol 1 No 1
doi: 10.2166/bgs.2019.198

Fabrication of flat-sheet TFC FO membranes

Preparation of FO membrane substrates via phase inversion

The casting solutions were composed of 16 wt.% CEC and various amounts of PVP K30, as shown in Table 1. The CEC and PVP were dissolved in DMAc and stirred by an orbital shaker at 60 °C for 24 h to obtain a homogeneous and transparent solution. Before casting, the prepared solution was left for degassing at room temperature for 24 h. About 10 mL casting solution was poured on a pre-cleaned glass plate, and was cast by a stainless-steel film applicator with a gap of 150 μm to form a 150 mm × 200 mm liquid membrane. After evaporation of the solvent for 30 s, the glass plate with the liquid membrane was immersed in a deionized water coagulation bath at room temperature to initiate phase inversion and form a solid substrate membrane. After sitting in the coagulation bath for 10 min, the obtained substrate was transferred into a flowing deionized water bath for 48 h to remove residual solvent before further use.

Table 1 | Compositions of the FO membrane substrates

Membrane ID	CEC (wt.%)	PVP (wt.%)	DMAc (wt.%)
M0	16.00	0.00	84.00
M0.5	16.00	0.50	83.50
M1	16.00	1.00	83.00
M2	16.00	2.00	82.00
M3	16.00	3.00	81.00
M4	16.00	4.00	80.00

Formation of the active layer via interfacial polymerization

The active layer of the TFC FO membrane was formed by IP on the surface of the CEC substrate (Zheng *et al.* 2018b). First, the pre-cast substrate membrane was soaked in an aqueous solution of 2 wt.% MPD for 120 s, and the excess MPD solution on the substrate surface was removed by blowing pure compressed nitrogen gas through an air knife. Subsequently, an 0.10 wt.% *n*-hexane solution of TMC was gently poured onto the MPD-soaked substrate surface and allowed to react with the residual MPD for 60 s, forming the PA active layer. After the TMC solution had drained off, the obtained TFC FO membrane was air-cured for 5 min. The resultant TFC FO membrane was rinsed with DI water to remove the residual solution and then stored in DI water before characterization and performance testing.

Membrane characterization

The pure water permeability (PWP) of the substrate membrane was measured using a cross-flow filtration setup, giving an effective membrane area of 11.34 cm^2. After 2 h of precompaction, a steady water flux was obtained under a pressure of 1.0 bar. The contact angles of the membrane substrates were measured by the sessile drop method, using a contact angle goniometer (DSA25, Kruss, Germany). Substrate samples were pre-dried in a vacuum at room temperature for 48 h. Droplets of DI water (2 μL) were applied onto a level membrane surface. At least five measurements were carried out at random locations on the top surface of the substrate. The membrane thickness (T) was measured by a digital micrometer (211-101, Sanliang, China) at five random locations on the samples. The porosity (ε) of the substrate was measured from the difference between wet and dry weight of a

Blue-Green Systems Vol 1 No 1
doi: 10.2166/bgs.2019.198

substrate sample by Equation (1) (Rabiee *et al.* 2015), where m_1, m_2, ρ, T, and A_m represent the wet weight, dry weight, the density of DI water, thickness, and effective area of the substrate sample. The average pore size (r_m) was calculated using the Gerout-Elford-Ferry equation (Equation (2)) (He *et al.* 2016), where η is the viscosity of water.

$$\varepsilon = \frac{m_1 - m_2}{\rho \times T \times A_m} \tag{1}$$

$$r_m = \sqrt{\frac{(2.9 - 1.75\varepsilon) \times 8 \times \eta \times T \times PWP}{\varepsilon}} \tag{2}$$

The mechanical properties of the CEC substrates were tested using a dynamic mechanical analyzer (DMA, Q800DE, TA, USA). The membrane samples were cut into strips of 8 mm width and 30 mm length. All tests were run at a ramp rate of 1 N/min at 25 °C.

The membrane morphologies were studied using a high-resolution field emission scanning electron microscope (HR-FESEM, Merlin, Carl Zeiss, Germany). The membrane substrates and TFC FO membranes were first dried by vacuum freeze drying for 48 h. The top surfaces, bottom surfaces, and cross sections of the membrane substrates and the top surfaces of TFC FO membranes were scanned. In particular, to observe cross sections of the membrane substrates, the samples were flash-frozen and cracked in liquid nitrogen.

Determination of membrane intrinsic properties

The water permeability (A), salt permeability (B), and structural parameter (S) are considered as the intrinsic properties of the FO membranes. The A value and B value were determined in the same filtration device applied to test the PWP of the substrates. The A value was tested by using DI water as the feed solution under the pressure of 5.0 bar. The A value was calculated using Equation (3) (Ghanbari *et al.* 2015b), where ΔV_a is the permeate volume in the water permeability test over a fixed time Δt_a, A_m is the effective area of the TFC membrane, ΔP is the transmembrane pressure difference:

$$A = \frac{\Delta V_a}{\Delta t_a \times A_m \times \Delta P} \tag{3}$$

The salt permeability (B) was calculated based on the salt rejection (Rs) and A value. Rs value was measured by using 2,000 ppm NaCl solution as the feed solution under the pressure of 5.0 bar. The Rs and B are calculated by Equations (4) and (5) (Ghanbari *et al.* 2015b), where C_f and C_p are the NaCl concentrations of feed and permeate solution, ΔP and $\Delta\pi$ are the transmembrane hydraulic and osmotic pressure differences:

$$R_S = \frac{C_f - C_p}{C_f} \times 100\% \tag{4}$$

$$B = A \times (\Delta P - \Delta\pi) \times \left(\frac{1}{R_S} - 1\right) \tag{5}$$

The structure parameter (S) can be estimated by the classical flux-fitting method with Equation (6) (Chen *et al.* 2017b), where D is the solute diffusion coefficient, π_{draw} and π_{feed} are the osmotic pressures of the draw solution and feed solution, J_W is the water flux under FO mode in performance test which is discussed in the section below.

$$S = \frac{D}{J_W}\left[\ln\frac{A \times \pi_{draw} + B}{A \times \pi_{feed} + J_W + B}\right] \tag{6}$$

Blue-Green Systems Vol 1 No 1
doi: 10.2166/bgs.2019.198

Forward osmosis performance experiments

FO experiments were conducted on a lab-scale cross-flow filtration setup. The effective membrane area in the FO cell was 12 cm^2 (2 cm × 6 cm). The FS and DS were circulated at the same fixed cross-flow rate of 480 mL/min on both sides of the FO membrane. A 1.0 M NaCl aqueous solution was used as the DS, while DI water was used as the FS. All FO performance experiments were evaluated under two operating modes: FO mode, where the active layer faced the FS, and pressure-retarded osmosis (PRO) mode, where the active layer faced the DS. Water flux was calculated by the weight changes of the DS recorded by a data-logging digital balance (AX4202ZH, Ohaus, USA). Meanwhile, the RSF was calculated from the change in concentration of the NaCl FS, as measured by a data-logging conductivity meter (DDSJ-308F, Rex, China). All tests were carried out at ambient temperature.

RESULTS AND DISCUSSION

Characterization of the CEC substrates

PVP was applied as a pore-foaming agent in the CEC substrate casting solution. Figure 2 summarizes the PWP values, contact angles, thicknesses, porosities, and average pore sizes of the CEC substrates with different PVP contents.

Figure 2(a) shows the thickness change of the CEC substrates with different PVP loadings. Although the gap height of casting applicator was 150 μm for all the CEC substrates, the thickness of the membranes was less than the gap height, ranging from 40 to 95 μm, after the phase inversion process. The thickness of the CEC substrates showed obvious growth with increasing PVP content from 0 to 4.0 wt.%. At higher PVP contents, a viscous casting solution with a low cloud point was formed. In other words, PVP increased the thermodynamic instability of the casting solution, which is considered to be a major contributor to the thickness of the phase inverted membrane (Han & Nam 2002).

The surface wetting characteristics of the substrate membranes were investigated by contact angle measurements. A lower value of contact angle indicates a more hydrophilic membrane surface. Figure 2(b) shows the change in the contact angle of the CEC substrates. Compared to the M0 substrate membrane, which had an average contact angle of 78.55°, the contact angles of the hydrophilic modified substrate membranes M0.5 to M4 declined from 72.82 to 64.37°. The result indicates that PVP improved the wettability of the CEC substrates because of improved porous top surfaces which is discussed in the following morphology study part.

Figure 2(c) illustrates the effect of PVP loading on the permeability of CEC substrates. The M0 substrate membrane, which contains no PVP, had a low PWP of 57.21 LMH/bar. On increasing the PVP loading to 2.0 wt.%, the PWP improved significantly to 362.22 LMH/bar. As the PVP loading increased, the water permeability of the CEC substrates improved markedly, which is ascribed to the PVP loading enhancing the porosity and hydrophilicity of the substrate membrane. However, on further increasing the PVP loading, the PWP rose only slightly from 362.22 LMH/bar for M2 to 431.83 LMH/bar for M4. The smaller increase in PWP on increasing the PVP loading could be a consequence of the continued thickening of the CEC substrates.

Figure 2(d) shows the porosity (ε) of the CEC substrates. Compared to the neat CEC membrane, PVP increased the porosity of the membranes. According to the experimental results, the value of ε increased from 73.48% for M0 to 83.40% for M2. However, the porosity barely increased when the PVP content increased from 2.0 to 4.0 wt.%. This phenomenon could be caused by two major factors. On the one hand, PVP, as a hydrophilic additive with non-solvent properties, could hasten the phase

Blue-Green Systems Vol 1 No 1
doi: 10.2166/bgs.2019.198

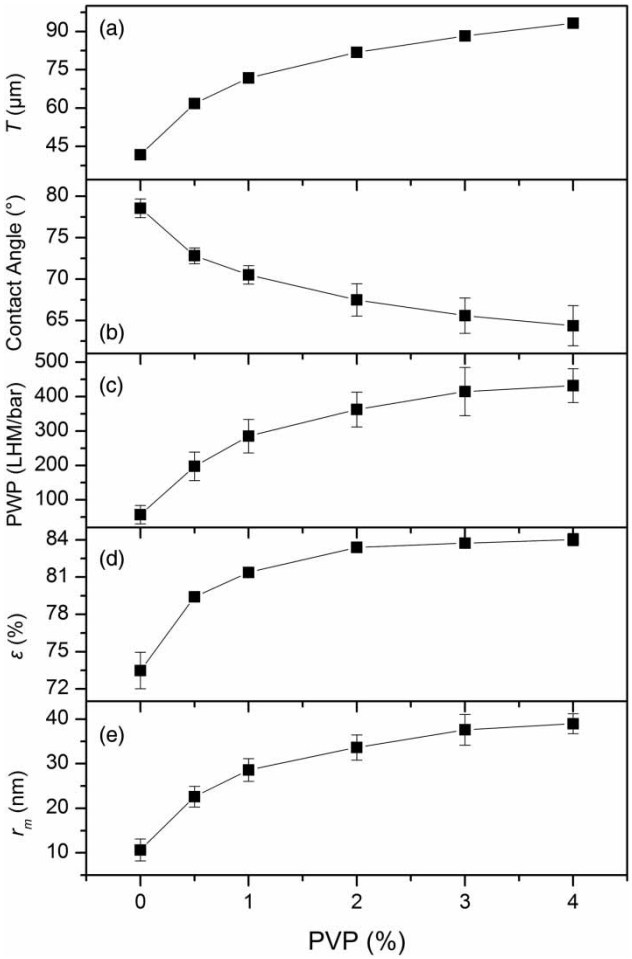

Figure 2 | Characteristics of CEC substrates with different PVP contents.

inversion and increase its intensity, resulting in the formation of more pores. On the other hand, excess PVP content could notably increase the viscosity of the casting solution, which could slow down the phase inversion rate and prevent the formation of pores (Han & Nam 2002; Anvari *et al.* 2016). Thus, the porosity surged when PVP content increased from 0 to 2.0 wt%, and stopped increasing when PVP content was over 2.0 wt%. For the same reason, a similar trend was observed in the average pore size (r_m) study of CEC substrates, which is shown in Figure 2(e). The value of r_m rose to 33.44 nm for M2 from 13.09 nm for M0 and increased to 39.26 nm for M4.

The mechanical properties are not crucial for the FO substrates because the FO process operates under normal pressures. However, the membrane must possess a reasonable mechanical strength for the practical use of the membrane in FO. The stress–strain curves of CEC substrates are shown in Figure 3. The stress–strain curves demonstrate that substrate M0 has the best tensile strength of the CEC substrates studied. The tensile strength declined obviously as the PVP content increased from 0 to 2%. The increasing porosity of the CEC substrates may be the cause of the reduction in strength. However, the tensile strength recovered slightly as the PVP content increased. There are two possible reasons for this result. First, the growth of the porosity slowed down when the PVP content was greater than 2%. Second, the thickness of CEC substrates increased with increasing PVP content.

Figure 4 shows the FESEM images of the cross sections, top surfaces, and bottom surfaces of the CEC substrates. According to the cross-section images, all CEC substrates exhibit typical asymmetric structures with finger-like pores formed under a thin sponge-like skin layer. However, the neat CEC

Blue-Green Systems Vol 1 No 1
doi: 10.2166/bgs.2019.198

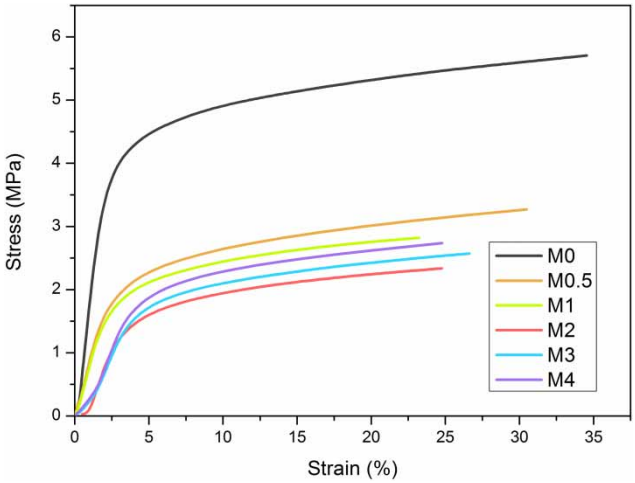

Figure 3 | Representative stress–strain curve of CEC substrates at different PVP content.

substrate has a remarkably different morphology to those of the PVP-modified substrates. First, the finger-like pores of the neat CEC substrate membrane are stumpier, even drop-like in shape. Meanwhile, a two-sublayer structure was observed in the modified substrates: a typical sublayer containing finger-like pores in the top part and macrovoids and a sponge-like wall sublayer in the bottom part. This results in the modified membranes having a more porous structure, which corresponds to the experimental results concerning the CEC substrate porosity. Finally, these cross-section images show the changes in the thickness of the substrates. The membrane thickness increases as the PVP content increases, which matches the thickness measurement results. As shown in the top surface images, the top surfaces have a dense morphology. This originates from the diffusion of the solvent from the cast-substrate membrane into the non-solvent, which could result in the polymer concentration at the top surface being higher than that at the underside, thus resulting in a denser top surface during the phase inversion process (Sahebi *et al.* 2016). However, the FESEM images do not show a difference in the top surfaces with different PVP contents. In contrast, the images of the bottom surfaces demonstrate the remarkably different character of the bottom surface compared to the top surface. As shown in the images, submicrometer pores were distributed on the bottom surface randomly. Furthermore, the density distribution of the submicrometer pores increases significantly with increasing PVP content.

Characteristics and performance of the TFC-FO membranes

TFC-FO membranes were prepared via interfacial polymerization to synthesize an active layer on the CEC substrates. The resultant TFC-FO membranes are labeled TFC-M0 to TFC-M4.

Figure 5 shows the top surface images of the TFC-FO membranes. However, both FESEM images and subsequent FO performance tests confirm that the active layer of the TFC-M0 membrane was not tightly bonded to the substrate membrane. At a low magnification of 100×, even by eye, obvious exfoliation of the active layer could be seen. On the other hand, TFC-M0.5 to TFC-M4 exhibited the typical 'ridge-and-valley'-like polyamide active layer at a magnification of 5,000×. Several previous investigations have tried to explain this phenomenon (Singh *et al.* 2006; Ghosh & Hoek 2009; Misdan *et al.* 2013; Liu & Ng 2015). First, according to the contact angle and porosity tests, the neat CEC membrane had poor hydrophilicity and wettability, which indicates that the neat CEC membrane cannot hold sufficient MPD aqueous solution to synthesize a tight active layer. Second, during the IP process, the MPD aqueous solution was kept inside the pores of the CEC substrates after the substrates were dried in the compressed nitrogen gas stream. In comparison with the neat CEC-substrate

Blue-Green Systems Vol 1 No 1
doi: 10.2166/bgs.2019.198

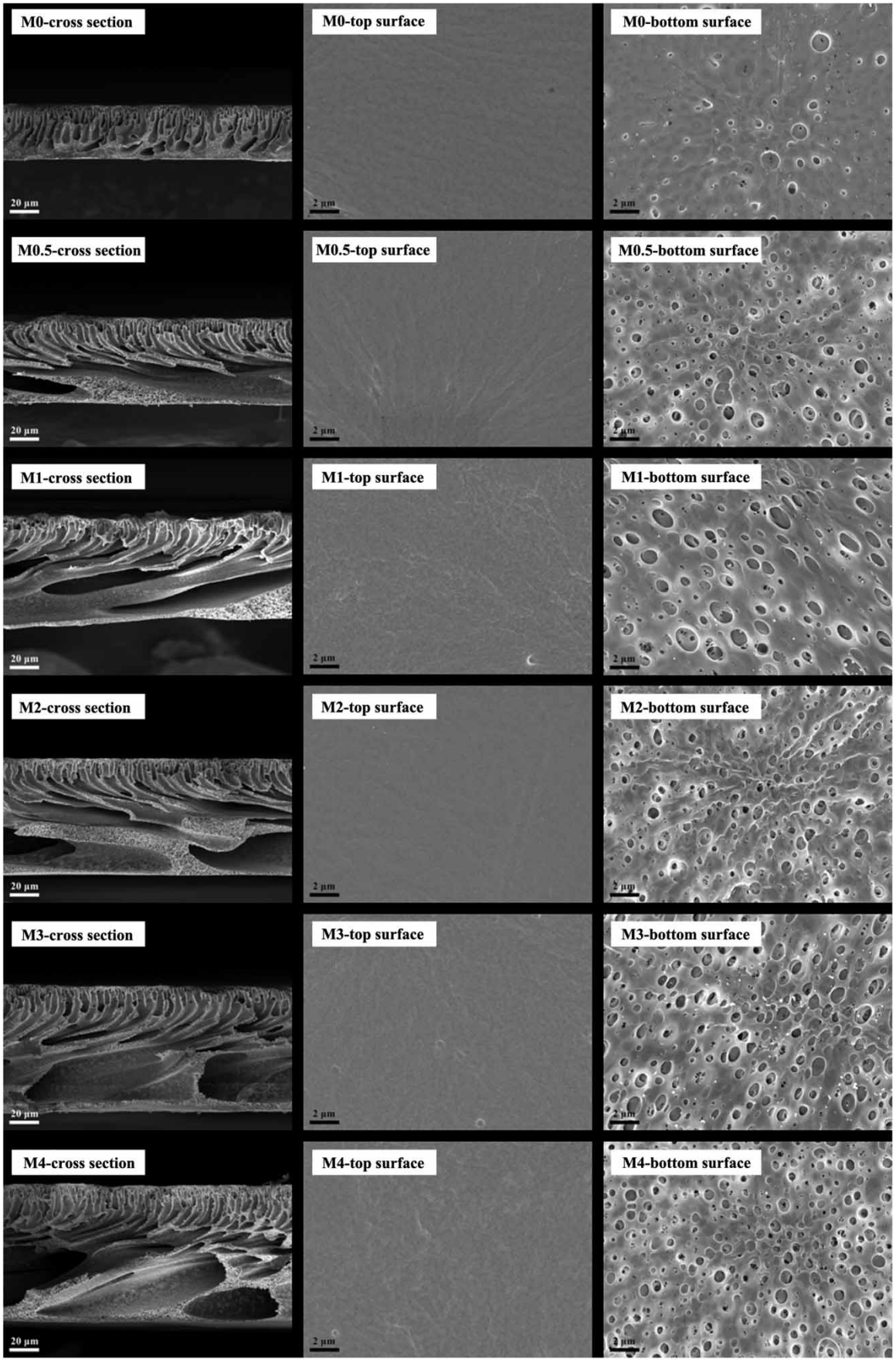

Figure 4 | FESEM images of CEC substrates with different PVP contents.

Blue-Green Systems Vol 1 No 1
doi: 10.2166/bgs.2019.198

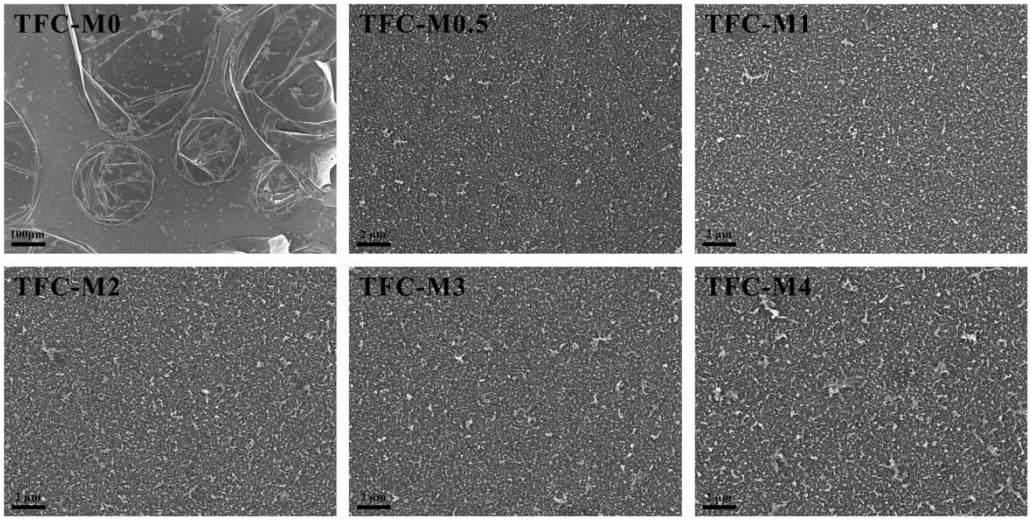

Figure 5 | FESEM images of the top surface of the TFC FO membranes.

membrane, the diffusion of residual MPD from the pores of the hydrophilic blend substrates was more difficult during the polymerization reaction. Thus, the polyamide formed inside the pores for the CEC/PVP-blend CEC substrates. However, the polyamide should have grown on top of the pores. Hence, the polyamide active layer was combined more tightly to the CEC/PVP substrates than the neat CEC substrate. This hypothesis reveals why the active layer synthesized on the neat CEC substrate membrane separated easily. Furthermore, because less MPD aqueous solution diffuses from the pores of the substrates as the PVP content increases, a relatively thinner and less cross-linked polyamide active layer was formed. This phenomenon leads to higher flux and salt passage as the membrane PVP content increases.

Water permeability (A), salt permeability (B), and structural parameter (S) are the intrinsic parameters to characterize the FO membranes, and the results are tabulated in Table 2. In particular, because of the obvious exfoliation of the active layer, the TFC-M0 cannot separate solute of draw solution and will not exhibit FO performance (Suwaileh *et al.* 2018). Consequently, the intrinsic parameters and FO performance of TFC-M0 will not be further discussed. According to the results, the A value and B value significantly improved with increasing PVP content. The reason for the improved hydrophilicity of the CEC substrates is because the thinner and less cross-linked active layer led to higher water flux and salt passage (Misdan *et al.* 2013). The lower value of the B/A ratio indicates a higher efficiency in reducing the RSF in the FO process. The B/A ratio increased slowly when PVP concentration was below 2.0 wt%, and then climbed appreciably. The S value reflects the membrane ICP during the FO process and has a positive correlation with the ICP (Wang *et al.* 2015). The results show that the S value significantly declined to 922 μm for TFC-M2 from 1,727 μm for TFC-M0.5, then slightly decreasing to 784 μm for TFC-M4. Taking comprehensive

Table 2 | Summary of calculated intrinsic properties of the TFC FO membranes

Membranes	*A* (LMH/bar)	*B* (LMH)	*B/A* (bar)	*S* (μm)
TFC-M0.5	0.63	0.08	0.13	1,727
TFC-M1	0.90	0.13	0.14	1,233
TFC-M2	1.17	0.20	0.17	922
TFC-M3	1.29	0.38	0.30	820
TFC-M4	1.24	0.48	0.39	784

Blue-Green Systems Vol 1 No 1
doi: 10.2166/bgs.2019.198

consideration of the B/A ratio and S value, TFC-M2 membrane seems to be the best candidate for FO process, and this will be further discussed in the following FO performance section.

The water flux and reverse salt flux were taken as two parameters to evaluate the performance of TFC-FO membranes. In particular, the water flux and reverse salt flux were extremely unstable arising from the obvious exfoliation of the active layer of TCF-M0. Consequently, the FO performance of TFC-M0 will not be discussed. Figure 6(a) shows the water fluxes of the TFC-M0.5 to TFC-M4 membranes under both FO mode and PRO mode using 1 M NaCl as the DS and DI water as the FS. The water flux is positively correlated with the PVP content in both FO and PRO modes. As shown in Figure 6(a), water flux under FO mode increased to 9.09 LMH for TFC-M2 and then slightly increased to 11.20 LHM for TFC-M4 from 4.35 LMH for TFC-M0.5. A similar trend was observed in PRO mode. The water flux under PRO mode soared to 20.67 LMH for TFC-M2 and then increased to 25.19 LHM for TFC-M4 from 9.87 LMH for TFC-M0.5. Furthermore, the water flux in PRO mode was significantly better than that in FO mode. This difference in performance is attributed to a different type and degree of ICP. In general, a highly dilutive ICP would reduce the osmosis driving force across the FO membrane and decrease the water flux in FO mode, while a slightly concentrative ICP occurs in PRO mode (Liu & Ng 2015).

Not only a high water flux but also a low RSF is an essential parameter to evaluate the performance of FO membranes. The RSF values of the TFC-M0.5 to TFC-M4 membranes in both FO mode and

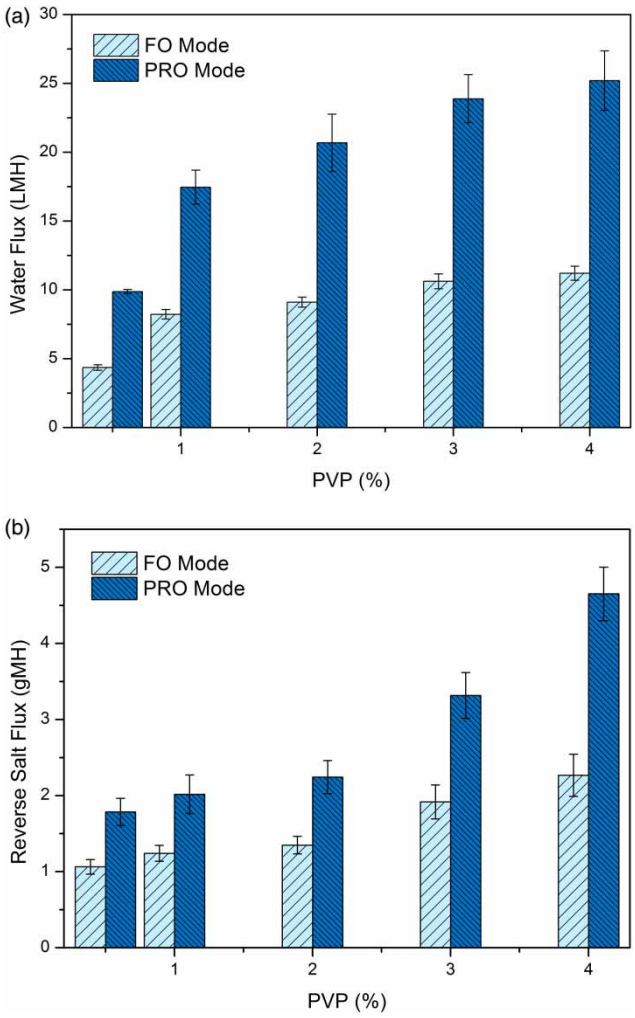

Figure 6 | FO Performance of TFC membranes with different PVP content: (a) water flux and (b) reverse salt flux under both FO and PRO modes with 1 M NaCl as DS and DI water as FS.

Blue-Green Systems Vol 1 No 1
doi: 10.2166/bgs.2019.198

PRO mode are shown in Figure 6(b). The RSF also increases with increasing PVP content, but its increasing trend is distinct from that of water flux. The RSF increased slightly to 1.35 gMH for TFC-M2 from 1.06 gMH for TFC-M0.5 and increased significantly, to 2.27 gMH, for TFC-M4. Likewise, a similar trend was observed in PRO mode. The RSF increased to 2.24 gMH for TFC-M2 from 1.79 gMH for TFC-M0.5 and rose to 4.65 gMH for TFC-M4. These results could be attributed to the thinner and less cross-linked active layer with higher PVP content, as discussed earlier. Furthermore, the high RSF could intensify the ICP, resulting in reduced water flux across the membranes (Sahebi *et al.* 2016). Hence, the increase in the water flux slows down with increasing PVP content.

The SRSF (ratio of RSF to water flux) has been identified as a metric to evaluate the osmotic process efficiency from the amount of draw solute loss per unit of water passed and to compare membrane performances for different membranes or draw solutes (Ren & McCutcheon 2015; Lim *et al.* 2017). High-performance FO membranes require high water flux and low RSF, i.e., a low SRSF value. Figure 7 shows the SRSF of the prepared TFC membranes in FO mode and PRO mode. The SRSF results show similar concave trends in both FO and PRO mode, reaching a minimum of 0.15 g/L in FO mode and 0.11 g/L in PRO mode at 2% PVP content. According to the earlier mentioned water flux and RSF data, the significantly increased water flux and slightly increased RSF at 0.5 to 2 wt.% PVP content contributed to the decline in SRSF, and the contrasting trends in water flux and RSF for 2 to 4 wt.% PVP content contributed to the increase in SRSF. The SRSF results are in good agreement with membrane intrinsic parameters' results. Taking comprehensive consideration

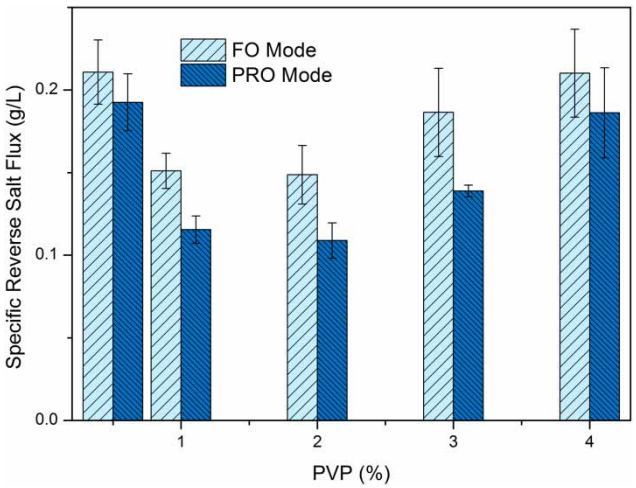

Figure 7 | Specific reverse salt flux for TFC membranes under both FO and PRO modes.

of FO performance and membrane intrinsic parameters' results, TFC-M2 should be the optimal FO membrane.

Comparison of FO performance with other FO membranes

Table 3 lists the FO performances of various lab-made flat-sheet TFC or TFN FO membranes and commercial HTI TFC FO membranes. Recently, PSF, PES, PVDF, and PAN have become common materials for the fabrication of substrates for TFC FO membranes (Widjojo *et al.* 2011; Ma *et al.* 2013; Tian *et al.* 2013; Shen *et al.* 2016). Because these polymers are hydrophobic, the membrane casting solution must be added to the pore-forming agent, such as PVP, LiCl, PEG, ethylene glycol, and ethanol (like P-1 to P-5), or blended with hydrophilic polymers and nanoparticles (like B-1 to B-4). According to the table, TFC-M2 and TFC-M4 have comparable levels of water flux and notably lower RSF compared to those of membranes P-1 to P-5 and the commercial HTI TFC membrane. Thus, all CEC-substrate TFC membranes exhibit better SRSF performance compared to the other TFC membranes.

Blue-Green Systems Vol 1 No 1
doi: 10.2166/bgs.2019.198

Table 3 | Comparison between the performance of the FO membranes prepared in this work and FO membranes prepared with other materials

No.	Basic polymer	Pore-forming agent	Blended polymer or nanoparticle	FS	DS	Water flux FO/PRO LMH	RSF FO/PRO gMH	SRSF FO/PRO g/L	Reference
TFC-M0.5	CEC	PVP	–	DI	1M NaCl	4.35/9.87	1.06/1.79	0.21/0.19	This work
TFC-M2	CEC	PVP	–	DI	1M NaCl	9.10/20.67	1.35/2.24	0.15/0.11	This work
TFC-M4	CEC	PVP	–	DI	1M NaCl	11.20/25.19	2.26/4.65	0.21/0.19	This work
P-1*	PSF	PVP, LiCl	–	DI	1M NaCl	11.01/25.71	5.49/9.34	0.50/0.36	Ma *et al.* (2013)
P-2	PSF	PVP	–	DI	2M NaCl	15.80/30.10	3.80/8.00	0.24/0.27	Emadzadeh *et al.* (2014)
P-3	PES	Ethylene glycol	–	DI	2M NaCl	10.50/13.50	3.10/3.70	0.30/0.27	Widjojo *et al.* (2011)
P-4	PVDF	–	–	DI	1M NaCl	11.60/30.40	3.50/6.40	0.30/0.21	Tian *et al.* (2013)
P-5*	PAN	Ethanol, LiCl	–	DI	2M NaCl	21.90/30.79	7.84/12.02	0.36/0.39	Shen *et al.* (2016)
B-1*	PSF	PVP, LiCl	Zeolite	DI	1M NaCl	30.23/64.71	18.22/38.43	0.60/0.59	Ma *et al.* (2013)
B-2	PSF	PVP	TiO_2	DI	2M NaCl	29.70/56.27	7.30/14.14	0.25/0.25	Emadzadeh *et al.* (2014)
B-3	PSF	–	LDH	DI	1M NaCl	18.10/34.60	8.10/12.70	0.45/0.37	Lu *et al.* (2016b)
B-4	PES	Ethylene glycol	PES-co-sPPSU	DI	2M NaCl	16.50/21.00	3.10/3.70	0.19/0.18	Widjojo *et al.* (2011)
C-1	Commercial HTI TFC membrane			DI	1M NaCl	15.10/30.05	4.40/11.20	0.29/0.37	Ren & McCutcheon (2014)

*The performance data of P-1, P-5, and B-1 were obtained through the figures from the corresponding literature.

CONCLUSION

In the study, CEC and PVP were chosen as the membranes' material and pore-forming agent to prepare substrates for TFC FO membranes, respectively. With increasing PVP content, the PWP, hydrophilicity, porosity, and average pore size of the substrates significantly improved. Visualization of the substrate morphologies showed that a two-sublayer substrate, a fringe-like top sublayer and a sponge-like bottom sublayer with macrovoids, was formed after the introduction of PVP. The optimization of the substrate properties improved the CEC membranes, making them more suitable TFC membrane substrates. However, the membrane thickness increased and the mechanical strength decreased after the addition of PVP. The surface images of the TFC membranes illustrate that the IP-formed polyamide active layer was exfoliated from the substrate containing no PVP. However, the FO membranes formed of PVP-modified substrates exhibited good FO performance. The TFC-M2 membrane exhibited a water flux of 9.10/20.67 LMH, 1.35/2.24 gMH RSF, and 0.15/0.11 g/L SRSF under FO/PRO mode while using 1 M NaCl as the DS and DI water as the FS. A comparison of FO performance with other FO membranes showed that the FO membranes with CEC substrates exhibited excellent SRSF performance. The results of this investigation clearly show that the PVP-optimized membranes can be used as substrates for TFC FO membranes.

ACKNOWLEDGEMENTS

Financial supports from the Ministry of Science and Technology of China for State Key Research and Development Project (2016YFC0400702), and the Department of Science and Technology of Guizhou Province (2017-5409) are gratefully acknowledged.

Blue-Green Systems Vol 1 No 1
doi: 10.2166/bgs.2019.198

REFERENCES

Akther, N., Sodiq, A., Giwa, A., Daer, S., Arafat, H. A. & Hasan, S. W. 2015 Recent advancements in forward osmosis desalination: a review. *Chemical Engineering Journal* **281**, 502–522.

Altaee, A., Sharif, A., Zaragoza, G. & Ismail, A. F. 2015 Evaluation of FO-RO and PRO-RO designs for power generation and seawater desalination using impaired water feeds. *Desalination* **368**, 27–35.

Ansari, A. J., Hai, F. I., Price, W. E., Drewes, J. E. & Nghiem, L. D. 2017 Forward osmosis as a platform for resource recovery from municipal wastewater – A critical assessment of the literature. *Journal of Membrane Science* **529**, 195–206.

Anvari, A., Safekordi, A., Hemmati, M., Rekabdar, F., Tavakolmoghadam, M., Yancheshme, A. A. & Gheshlaghi, A. 2016 Enhanced separation performance of PVDF/PAN blend membrane based on PVP tuning. *Desalination and Water Treatment* **57** (26), 12090–12098.

Bui, N.-N. & McCutcheon, J. R. 2016 Nanoparticle-embedded nanofibers in highly permselective thin-film nanocomposite membranes for forward osmosis. *Journal of Membrane Science* **518**, 338–346.

Chekli, L., Phuntsho, S., Kim, J. E., Kim, J., Choi, J. Y., Choi, J.-S., Kim, S., Kim, J. H., Hong, S., Sohn, J. & Shon, H. K. 2016 A comprehensive review of hybrid forward osmosis systems: performance, applications and future prospects. *Journal of Membrane Science* **497**, 430–449.

Chen, G. E., Sun, W. G., Wu, Q., Kong, Y. F., Xu, Z. L., Xu, S. J. & Zheng, X. P. 2017a Effect of cellulose triacetate membrane thickness on forward-osmosis performance and application for spent electroless nickel plating baths. *Journal of Applied Polymer Science* **134** (28), 10.

Chen, G., Liu, R., Shon, H. K., Wang, Y., Song, J., Li, X.-M. & He, T. 2017b Open porous hydrophilic supported thin-film composite forward osmosis membrane via co-casting for treatment of high-salinity wastewater. *Desalination* **405**, 76–84.

Chen, X., Xu, J., Lu, J., Shan, B. & Gao, C. 2017c Enhanced performance of cellulose triacetate membranes using binary mixed additives for forward osmosis desalination. *Desalination* **405**, 68–75.

Elimelech, M. & Phillip, W. A. 2011 The future of seawater desalination: energy, technology, and the environment. *Science* **333** (6043), 712–717.

Emadzadeh, D., Lau, W. J., Matsuura, T., Rahbari-Sisakht, M. & Ismail, A. F. 2014 A novel thin film composite forward osmosis membrane prepared from PSf-TiO_2 nanocomposite substrate for water desalination. *Chemical Engineering Journal* **237**, 70–80.

Ghanbari, M., Emadzadeh, D., Lau, W. J., Lai, S. O., Matsuura, T. & Ismail, A. F. 2015a Synthesis and characterization of novel thin film nanocomposite (TFN) membranes embedded with halloysite nanotubes (HNTs) for water desalination. *Desalination* **358**, 33–41.

Ghanbari, M., Emadzadeh, D., Lau, W. J., Matsuura, T., Davoody, M. & Ismail, A. F. 2015b Super hydrophilic TiO_2/HNT nanocomposites as a new approach for fabrication of high performance thin film nanocomposite membranes for FO application. *Desalination* **371**, 104–114.

Ghosh, A. K. & Hoek, E. M. V. 2009 Impacts of support membrane structure and chemistry on polyamide-polysulfone interfacial composite membranes. *Journal of Membrane Science* **336** (1–2), 140–148.

Han, M.-J. & Nam, S.-T. 2002 Thermodynamic and rheological variation in polysulfone solution by PVP and its effect in the preparation of phase inversion membrane. *Journal of Membrane Science* **202** (1–2), 55–61.

He, M., Fan, X., Yang, Z., Zhang, R., Liu, Y., Fan, L., Zhang, Q., Su, Y. & Jiang, Z. 2016 Antifouling high-flux membranes via surface segregation and phase separation controlled by the synergy of hydrophobic and hydrogen bond interactions. *Journal of Membrane Science* **520**, 814–822.

Heikkinen, J., Kyllonen, H., Jarvela, E., Gronroos, A. & Tang, C. Y. 2017 Ultrasound-assisted forward osmosis for mitigating internal concentration polarization. *Journal of Membrane Science* **528**, 147–154.

Huang, M., Meng, L., Li, B., Niu, F., Lv, Y., Deng, Q. & Li, J. 2019 Fabrication of innovative forward osmosis membranes via multilayered interfacial polymerization on electrospun nanofibers. *Journal of Applied Polymer Science* **136** (12), 47247.

Joshi, G., Naithani, S., Varshney, V. K., Bisht, S. S. & Rana, V. 2017 Potential use of waste paper for the synthesis of cyanoethyl cellulose: a cleaner production approach towards sustainable environment management. *Journal of Cleaner Production* **142**, 3759–3768.

Li, D., Yan, Y. & Wang, H. 2016 Recent advances in polymer and polymer composite membranes for reverse and forward osmosis processes. *Progress in Polymer Science* **61**, 104–155.

Lim, S., Park, M. J., Phuntsho, S., Tijing, L. D., Nisola, G. M., Shim, W.-G., Chung, W.-J. & Shon, H. K. 2017 Dual-layered nanocomposite substrate membrane based on polysulfone/graphene oxide for mitigating internal concentration polarization in forward osmosis. *Polymer* **110**, 36–48.

Ling, M. M. & Chung, T.-S. 2011 Novel dual-stage FO system for sustainable protein enrichment using nanoparticles as intermediate draw solutes. *Journal of Membrane Science* **372** (1–2), 201–209.

Liu, X. & Ng, H. Y. 2015 Fabrication of layered silica-polysulfone mixed matrix substrate membrane for enhancing performance of thin-film composite forward osmosis membrane. *Journal of Membrane Science* **481**, 148–163.

Liu, Y., Huang, H. T., Huo, P. F. & Gu, J. Y. 2017 Exploration of zwitterionic cellulose acetate antifouling ultrafiltration membrane for bovine serum albumin (BSA) separation. *Carbohydrate Polymers* **165**, 266–275.

Lu, P., Liang, S., Zhou, T., Mei, X., Zhang, Y., Zhang, C., Umar, A., Wang, H. & Wang, Q. 2016a Typical thin-film composite (TFC) membranes modified with inorganic nanomaterials for forward osmosis: a review. *Nanoscience and Nanotechnology Letters* **8** (11), 906–916.

Blue-Green Systems Vol 1 No 1
doi: 10.2166/bgs.2019.198

Lu, P., Liang, S., Qiu, L., Gao, Y. & Wang, Q. 2016b Thin film nanocomposite forward osmosis membranes based on layered double hydroxide nanoparticles blended substrates. *Journal of Membrane Science* **504**, 196–205.

Ma, N., Wei, J., Qi, S., Zhao, Y., Gao, Y. & Tang, C. Y. 2013 Nanocomposite substrates for controlling internal concentration polarization in forward osmosis membranes. *Journal of Membrane Science* **441**, 54–62.

Misdan, N., Lau, W. J., Ismail, A. F. & Matsuura, T. 2013 Formation of thin film composite nanofiltration membrane: effect of polysulfone substrate characteristics. *Desalination* **329**, 9–18.

Morales-Torres, S., Esteves, C. M. P., Figueiredo, J. L. & Silva, A. M. T. 2016 Thin-film composite forward osmosis membranes based on polysulfone supports blended with nanostructured carbon materials. *Journal of Membrane Science* **520**, 326–336.

Qasim, M., Darwish, N. A., Sarp, S. & Hilal, N. 2015 Water desalination by forward (direct) osmosis phenomenon: a comprehensive review. *Desalination* **374**, 47–69.

Rabiee, H., Vatanpour, V., Farahani, M. H. D. A. & Zarrabi, H. 2015 Improvement in flux and antifouling properties of PVC ultrafiltration membranes by incorporation of zinc oxide (ZnO) nanoparticles. *Separation and Purification Technology* **156**, 299–310.

Ren, J. & McCutcheon, J. R. 2014 A new commercial thin film composite membrane for forward osmosis. *Desalination* **343**, 187–193.

Ren, J. & McCutcheon, J. R. 2015 Polyacrylonitrile supported thin film composite hollow fiber membranes for forward osmosis. *Desalination* **372**, 67–74.

Sahebi, S., Phuntsho, S., Woo, Y. C., Park, M. J., Tijing, L. D., Hong, S. & Shon, H. K. 2016 Effect of sulphonated polyethersulfone substrate for thin film composite forward osmosis membrane. *Desalination* **389**, 129–136.

Sant'Anna, V., Gurak, P. D., de Vargas, N. S., da Silva, M. K., Ferreira Marczak, L. D. & Tessaro, I. C. 2016 Jaboticaba (Myrciaria jaboticaba) juice concentration by forward osmosis. *Separation Science and Technology* **51** (10), 1708–1715.

Shen, L., Xiong, S. & Wang, Y. 2016 Graphene oxide incorporated thin-film composite membranes for forward osmosis applications. *Chemical Engineering Science* **143**, 194–205.

Singh, P. S., Joshi, S. V., Trivedi, J. J., Devmurari, C. V., Rao, A. P. & Ghosh, P. K. 2006 Probing the structural variations of thin film composite RO membranes obtained by coating polyamide over polysulfone membranes of different pore dimensions. *Journal of Membrane Science* **278** (1–2), 19–25.

Suwaileh, W. A., Johnson, D. J., Sarp, S. & Hilal, N. 2018 Advances in forward osmosis membranes: altering the sub-layer structure via recent fabrication and chemical modification approaches. *Desalination* **436**, 176–201.

Teramoto, Y. 2015 Functional thermoplastic materials from derivatives of cellulose and related structural polysaccharides. *Molecules* **20** (4), 5487–5527.

Tian, M., Qiu, C., Liao, Y., Chou, S. & Wang, R. 2013 Preparation of polyamide thin film composite forward osmosis membranes using electrospun polyvinylidene fluoride (PVDF) nanofibers as substrates. *Separation and Purification Technology* **118**, 727–736.

Wang, Y. & Xu, T. 2015 Anchoring hydrophilic polymer in substrate: an easy approach for improving the performance of TFC FO membrane. *Journal of Membrane Science* **476**, 330–339.

Wang, Y., Ou, R., Wang, H. & Xu, T. 2015 Graphene oxide modified graphitic carbon nitride as a modifier for thin film composite forward osmosis membrane. *Journal of Membrane Science* **475**, 281–289.

Widjojo, N., Chung, T.-S., Weber, M., Maletzko, C. & Warzelhan, V. 2011 The role of sulphonated polymer and macrovoid-free structure in the support layer for thin-film composite (TFC) forward osmosis (FO) membranes. *Journal of Membrane Science* **383** (1–2), 214–223.

Wu, Y., Zhu, H., Feng, L. & Zhang, L. 2016 Effects of polyethylene glycol on the structure and filtration performance of thin-film PA-Psf composite forward osmosis membranes. *Separation Science and Technology* **51** (5), 862–873.

Zhang, X., Tian, J., Ren, Z., Shi, W., Zhang, Z., Xu, Y., Gao, S. & Cui, F. 2016 High performance thin-film composite (TFC) forward osmosis (FO) membrane fabricated on novel hydrophilic disulfonated poly(arylene ether sulfone) multiblock copolymer/polysulfone substrate. *Journal of Membrane Science* **520**, 529–539.

Zheng, K., Zhou, S. & Zhou, X. 2018a High-performance thin-film composite forward osmosis membrane fabricated on low-cost PVB/PVC substrate. *New Journal of Chemistry* **42** (16), 13382–13392.

Zheng, K., Zhou, S. & Zhou, X. 2018b A low-cost and high-performance thin-film composite forward osmosis membrane based on an SPSU/PVC substrate. *Scientific Reports* **8** (1), 10022.

Zhou, J., Li, Q., Song, Y., Zhang, L. & Lin, X. 2010 A facile method for the homogeneous synthesis of cyanoethyl cellulose in NaOH/urea aqueous solutions. *Polymer Chemistry* **1** (10), 1662–1668.

Zhou, Z., Lee, J. Y. & Chung, T.-S. 2014 Thin film composite forward-osmosis membranes with enhanced internal osmotic pressure for internal concentration polarization reduction. *Chemical Engineering Journal* **249**, 236–245.

First received 15 April 2019; accepted in revised form 30 June 2019. Available online 19 July 2019